MATERIALS SCIENCE

Synthetic WSe_2 monolayers with high photoluminescence quantum yield

Hyungjin Kim[1,2]*, Geun Ho Ahn[1,2]*, Joy Cho[1,2], Matin Amani[1,2], James P. Mastandrea[2,3], Catherine K. Groschner[2,3,4], Der-Hsien Lien[1,2], Yingbo Zhao[1,2], Joel W. Ager III[2,3], Mary C. Scott[2,3,4], Daryl C. Chrzan[2,3], Ali Javey[1,2†]

In recent years, there have been tremendous advancements in the growth of monolayer transition metal dichalcogenides (TMDCs) by chemical vapor deposition (CVD). However, obtaining high photoluminescence quantum yield (PL QY), which is the key figure of merit for optoelectronics, is still challenging in the grown monolayers. Specifically, the as-grown monolayers often exhibit lower PL QY than their mechanically exfoliated counterparts. In this work, we demonstrate synthetic tungsten diselenide (WSe_2) monolayers with PL QY exceeding that of exfoliated crystals by over an order of magnitude. PL QY of ~60% is obtained in monolayer films grown by CVD, which is the highest reported value to date for WSe_2 prepared by any technique. The high optoelectronic quality is enabled by the combination of optimizing growth conditions via tuning the halide promoter ratio, and introducing a simple substrate decoupling method via solvent evaporation, which also mechanically relaxes the grown films. The achievement of scalable WSe_2 with high PL QY could potentially enable the emergence of technologically relevant devices at the atomically thin limit.

INTRODUCTION

Two-dimensional (2D) transition metal dichalcogenides (TMDCs) have demonstrated immense potential for optoelectronics and sub–10-nm transistors (*1*–*3*). TMDCs have natural out-of-plane self-terminating surfaces without dangling bonds, although defects exist (*4*). Furthermore, near-unity photoluminescence quantum yield (PL QY) has been demonstrated in mechanically exfoliated sulfur-based TMDCs, namely, MoS_2 and WS_2, by using bis(trifluoromethane) sulfonamide (TFSI) treatment (*5*, *6*). The achievement of high PL QY indicates that the TMDC monolayers are well suited for high-performance optoelectronics at the atomically thin limit.

Large-area growth of high-quality TMDC monolayers is essential to translate their unique properties into practical devices. In this regard, various growth techniques have been reported in the literature, including sulfurization/selenization of oxide films (*7*, *8*), chemical vapor deposition (CVD) (*9*–*11*), and metal organic CVD (*12*). This research has now progressed to the growth of wafer-scale monolayer films (*13*). Furthermore, direct synthesis of vertical and lateral heterostructures (*14*, *15*), spatially controlled synthesis of full atomically thin circuitry (*16*), and strain-engineered growth of 2D materials (*17*) have been demonstrated. However, the grown monolayers exhibit inferior optoelectronic performance compared with micromechanically exfoliated materials. Specifically, the PL QY of the grown films is often lower than their mechanically exfoliated counterparts (*18*–*22*). This presents a major challenge for the realization of high-performance TMDC optoelectronics, where PL QY is the key figure of merit for determining the eventual device characteristics (*23*, *24*).

In this work, we report CVD growth of tungsten diselenide (WSe_2) monolayers with PL QY of 60% at low injection levels, which is the highest reported to date for WSe_2 and an order of magnitude higher than what is obtained from exfoliated films (*6*, *17*). Moreover, the samples exhibit a PL QY of 12% at high injection levels. This high-pump PL QY is 20 times higher than the previously reported values for any TMDC monolayer, including TFSI-treated MoS_2 (*5*, *24*–*26*). Detailed optical characterizations of the grown WSe_2 monolayers are performed, and we find that the strong coupling to the substrate of as-grown monolayers inhibits probing the intrinsic properties. Using a solvent evaporation–mediated decoupling (SEMD) process, we demonstrate reduced nonradiative recombination and higher PL QY in the grown monolayers by decoupling from the substrate. In parallel, we find that halide-based growth promoters play a substantial role in synthesizing optimal material quality.

RESULTS AND DISCUSSION

WSe_2 monolayers grown via CVD have strong interactions with the substrate. We and others have used this effect for controlled strain engineering of the grown monolayers based on the thermal coefficient of expansion mismatch between the substrate and the monolayer (*27*, *28*). The substrate coupling and the strain can be released by using poly(methyl methacrylate)–mediated transfer of the monolayer onto a secondary substrate. However, this process often requires harsh environments, i.e., hydrofluoric acid, potassium hydroxide, or the use of sonication to detach the monolayer from the substrate. Complete removal of the polymer used for transfer is also challenging and often requires subsequent thermal annealing of the sample.

As a less damaging alternative, we developed the SEMD process to decouple grown monolayers from the substrate (Fig. 1A). The process is very simple and begins by placing a droplet of solvent with high vapor pressure (e.g., acetone) on an as-grown WSe_2 monolayer.

As the solvent evaporates, the surface tension pulls on the grown material and decouples the material from the substrate. A balance of forces allows the process to decouple the monolayer, as described later in the manuscript.

The effect of SEMD was characterized by PL spectroscopy. We find that the emission peak blue shifts by ~80 meV from 1.57 eV for the

[1]Department of Electrical Engineering and Computer Sciences, University of California at Berkeley, Berkeley, CA 94720, USA. [2]Materials Sciences Division, Lawrence Berkeley National Laboratory, Berkeley, CA 94720, USA. [3]Department of Materials Science and Engineering, University of California at Berkeley, Berkeley, CA 94720, USA. [4]National Center for Electron Microscopy, Molecular Foundry, Lawrence Berkeley National Laboratory, Berkeley, CA 94720, USA.
*These authors contributed equally to this work.
†Corresponding author. Email: ajavey@berkeley.edu

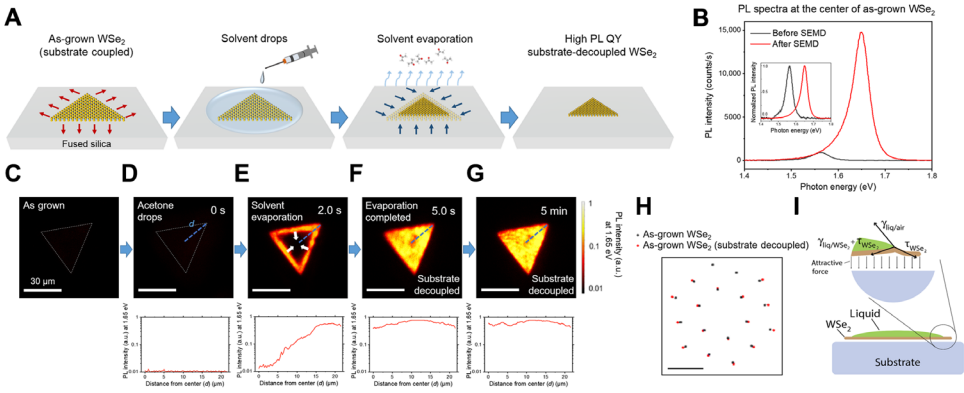

Fig. 1. Synthetic WSe_2 monolayer with high PL QY after SEMD. (**A**) Schematic of the SEMD process. An as-grown WSe_2 monolayer is immersed in a droplet of solvent. During the solvent evaporation, the substrate decoupling process of the WSe_2 monolayer is accomplished with the enhanced PL QY. (**B**) PL spectra measured at the center of an as-grown WSe_2 monolayer with an excitation power of 15 W cm^{-2} before and after the SEMD process; inset shows normalized spectra. (**C** to **G**) In situ PL imaging of the SEMD process in a WSe_2 monolayer. Scale bars, 30 μm (for all PL images). Note that the images were taken using a 1.65-eV bandpass filter that blocks the emission from the as-grown monolayer and plotted on a logarithmic scale. PL intensity profile across the WSe_2 monolayer is presented in the bottom plots. PL images at additional timestamps are shown in fig. S1. a.u., arbitrary units. (**H**) Overlay of diffraction spots for as-grown and substrate-decoupled samples; 1.54 ± 0.05% tensile strain in the as-grown sample is released after the SEMD process. Scale bar, 5 nm^{-1}. Original diffraction patterns of the samples are shown in fig. S5. (**I**) Schematic describing the factors influencing the SEMD process of the WSe_2 monolayer.

as-grown sample to 1.65 eV after SEMD (Fig. 1B). The post-SEMD emission peak position closely matches that of unstrained CVD WSe_2 monolayers and that of micromechanically exfoliated samples (*20*, *29*), indicating the full release of the built-in strain and, thus, complete decoupling of the synthetic monolayer from the substrate. Critically, the substrate-decoupled WSe_2 monolayers exhibit more than an order of magnitude brighter PL emission intensity compared with substrate-coupled as-grown monolayers before SEMD. To further investigate the SEMD mechanism, we performed in situ PL imaging as the solvent evaporates (Fig. 1, C to G, and fig. S1). Imaging was performed using a bandpass filter centered at 1.65 eV, which blocks the emission of the substrate-coupled as-grown sample under biaxial tensile strain. Before and immediately after dispensing of the solvent, we observed no strong emission, as can be seen in Fig. 1 (C and D). In addition, in situ PL spectra measurement in acetone baths (fig. S2) shows no change in PL intensity or spectra unlike the changes observed in Fig. 1B. This suggests that the presence of the solvent by itself does not influence the built-in substrate coupling in as-grown samples. However, at the onset of solvent evaporation from the monolayer, we start to observe strong emission at 1.65 eV at the edge of the crystal (Fig. 1E). Once the solvent is fully evaporated (Fig. 1F), the emission becomes uniform over the full sample domain (Fig. 1G). As plotted in Fig. 1 (C to G) and fig. S1, the PL intensity profile across the WSe_2 monolayer shows that the PL intensity at 1.65 eV starts to increase from the edge and becomes uniformly enhanced over the SEMD process. This indicates that the substrate decoupling is mediated by the solvent evaporation and is initiated from the edges of the monolayer. Subsequently, the emission remains stable over time. It is worth noting that the SEMD process is also applicable to other growth substrates, including sapphire (fig. S3). For this work, we primarily focused on using acetone as the solvent, given its high vapor pressure and minimal effects to the grown material quality (*30*). Other solvents with varying vapor pressures were also investigated and show similar decoupling results (fig. S4).

We used transmission electron microscopy (TEM) electron diffraction to directly measure the lattice constant of the grown WSe_2 before and after SEMD to verify the release of biaxial tensile strain of the as-grown films. WSe_2 monolayers were prepared via direct growth on SiO_2 membranes, and the SEMD process was performed on these samples. Figure 1H shows the overlay of diffraction spots for the as-grown and substrate-decoupled WSe_2 monolayers. We calculated the diffraction spots as the center of mass of individual diffraction spots from the measurements shown in fig. S5. All the electron diffraction measurements for as-grown WSe_2 were taken with the identical lens settings, so as not to alter the calibration of the camera length and the lens aberrations. A polycrystalline Cu standard was used for the calibration. From the electron diffraction measurements and the subsequent comparison of lattice constants from each of the diffraction patterns, we find that ~1.54 ± 0.05% tensile strain was released from the as-grown WSe_2 monolayer after SEMD. The strain value in the as-grown films is consistent with our previous study using similar growth conditions. Note that the diffraction pattern of an as-exfoliated WSe_2 monolayer is also shown in fig. S5. Here, the calculated lattice constant value from the exfoliated sample matches that of substrate-decoupled WSe_2, verifying the complete release of built-in strain after the SEMD process.

While the development of a detailed understanding of the process awaits further study, we propose the following model as a guide to understand the experimental results. First, assume that the experimentally observed intrinsic biaxial tensile strain from growth is stabilized by the friction-induced resistance to sliding of the monolayer on the substrate. There might be, of course, local pinning sites that more strongly couple the film and substrate, and these would change the details of the strain relief process, but friction will still play a role. Typically, one expects that the friction force is proportional to the contact force between the film and substrate and that a reduced contact force would allow for the relaxation of the strain present in the as-grown monolayer. The geometry of a free-standing thin film with a droplet placed on it has been the subject of some studies (*31*–*34*). In the mechanism considered here, the interaction of the film with the substrate and the imposed biaxial strain in the film must be considered. Figure 1I illustrates the structure of the droplet as it evaporates, and it shows forces acting on the system near the triple point (junction of liquid, air, and WSe_2). For the process, the interfacial energy of the liquid/air

junction ($\gamma_{liq/air}$), the interfacial energy of the liquid/WSe_2 (γ_{liq/WSe_2}), the stress in the WSe_2 monolayer itself (γ_{WSe_2}), and the attractive force between the substrate and the WSe_2 are considered. The resulting forces can be balanced only if the monolayer is slightly raised from the substrate at the triple point, as shown in Fig. 1I, and it is hypothesized that this reduces the contact force between the film and the substrate. This reduction in friction would enable the local strain relief of the monolayer, as the distortion of the film is expected to be localized to the region of the triple point. It is expected that once the triple point has passed a region, the film re-adheres to the substrate. Therefore, for larger films, one pass of the triple point may be insufficient to completely relax the strain, and multiple passes may be required.

We also investigated the effect of solvent evaporation on exfoliated WSe_2 monolayer samples, which are mechanically relaxed as processed. As shown in fig. S6, we used different WSe_2 crystals from three different vendors and found that the process has no significant effect on the exfoliated monolayers. Specifically, we observed minimal change in the emission intensity and peak position. The substrate-decoupled monolayers are also stable after acetone evaporation. As shown in fig. S7, the PL characteristic is stable after rinsing with various solvents, under vacuum, and over time in a humid condition. The results show that acetone does not chemically modify the monolayers and does not by itself affect the recombination processes. Instead, acetone evaporation induces surface tension–mediated decoupling of the monolayer.

In parallel, optimized growth conditions are important for obtaining high PL QY. We find the role of the growth promoter particularly critical. In our case, a halide-based promoter was found to be essential to obtain WSe_2 with grain sizes on the order of 100 μm, as well as continuous films. Previous studies have shown that halide-based salts result in the formation of volatile tungsten-based halide species due to a chemical reaction between the tungsten oxide precursor and the alkali metal halides (*35*, *36*). We highlighted the role of the halide promoter (KBr for this work) on the PL QY of the monolayer films in Fig. 2A by varying the KBr-to-WO_3 precursor weight ratio. For the explored range, no significant effect is observed on the PL QY as a function of KBr content for as-grown monolayers. By decoupling the monolayers, the intrinsic properties of the material can be assessed, following which, the strong effect of KBr weight ratio on the PL QY is observed (Fig. 2A). We find that in the case of higher promoter weight ratio (2:1, KBr:WO_3), the overall average PL QY after SEMD is one order of magnitude lower than that of samples grown with lower KBr amount (1:2; KBr:WO_3), while there was no WSe_2 growth if the promoter weight ratio was further reduced to 1:4, KBr:WO_3. Subsequently, all characterizations are performed on samples prepared with 1:2, KBr:WO_3.

Figure 2 (B and C) depicts the histograms of the low-pump (2 W cm^{-2}) PL QY and the emission peak position, respectively, for exfoliated WSe_2 monolayers and WSe_2 monolayers grown using optimized growth condition, before and after SEMD. We observed no statistically

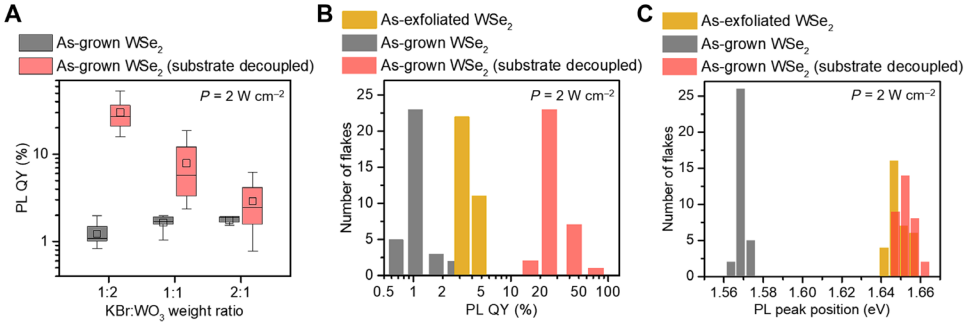

Fig. 2. PL of synthetic WSe_2 monolayer with optimized growth conditions after SEMD. (**A**) Box and whisker plot showing the PL QY of synthetic WSe_2 grown using varying promoter weight ratios both before and after the SEMD process. Error bars indicate SD of PL QY obtained from 10 different locations on the samples from the same growth. Histogram showing the (**B**) PL QY and (**C**) PL peak position of as-grown WSe_2 monolayers before and after the SEMD process and exfoliated WSe_2 monolayers. PL QY of as-exfoliated samples prepared from bulk crystals provided by three different vendors is shown in fig. S6.

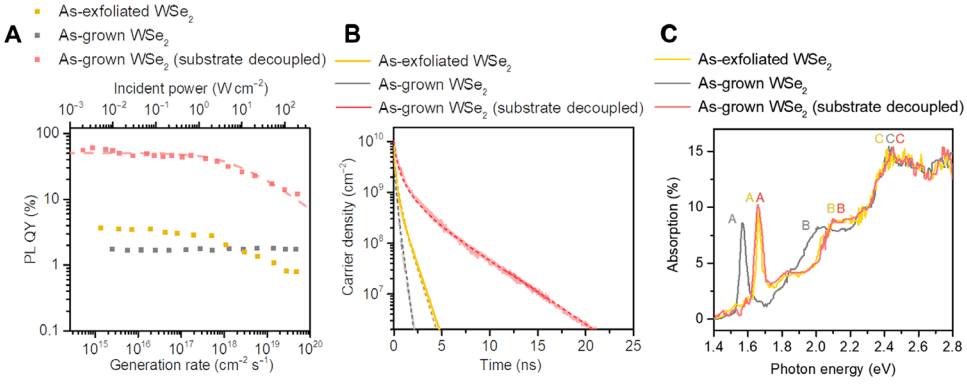

Fig. 3. Optical characterization. (**A**) Pump power dependence, (**B**) TRPL decay, and (**C**) absorption spectra of as-grown, substrate-decoupled, and as-exfoliated WSe_2 monolayers. Dashed line in generation rate–dependent PL QY curve is used to fit the recombination model described in Eq. 1. Dashed lines in TRPL decay show the fit to the dynamic model using parameters extracted from the steady-state experiment. Additional TRPL decay curves are shown in fig. S8.

significant difference for the emission peak position of the monolayer after SEMD and exfoliated WSe_2 monolayers. On the other hand, the as-grown samples consistently show an ~80-meV red shift due to tensile strain, which is consistent with the previous report (*17*). The PL QY of as-grown WSe_2 (1.4%) is slightly lower than that of exfoliated samples (3.1%). The grown monolayers after SEMD on the other hand show an average PL QY of 31.2%, with the highest observed value of 60%. This represents the highest PL QY reported in WSe_2 prepared by any method.

The reduction in PL when the sample is strongly coupled to the substrate may be attributed to a number of factors. As shown in Fig. 1H, TMDCs grown via the CVD method have intrinsic strain owing to the thermal expansion mismatch between the substrate and the material at the high growth temperature (*17*, *26*, *27*). This intrinsic strain results in modification of the band structure, which could affect its recombination dynamics. Theoretical calculations of band structure as a function of strain show that high biaxial tensile strain in the WSe_2 monolayer leads to indirect bandgap transition (*37*). Therefore, the band structure modification from intrinsic biaxial tensile strain can possibly reduce the PL of the as-grown WSe_2 monolayer. However, it is important to note that the exact band structure of TMDCs is yet to be understood. In addition to the impact of band structure change, the quenched PL in the as-grown samples could be a result of the close coupling to the surface roughness of fused silica or electronic coupling between the semiconductor and the substrate (*38*).

The dependence of the PL QY as a function of the excitation intensity (i.e., generation rate) is shown in Fig. 3A for an exfoliated monolayer and a CVD monolayer before and after SEMD. The data depict the dramatic enhancement of PL QY on the SEMD process at the generation rates spanning six orders of magnitudes. The QY exhibits a sublinear excitation pump power dependence with a peak value of 60% at the low generation rates, followed by a drop at high generation rates (>~10^{18} cm^{-2} s^{-1}). The recombination kinetics of the TMDCs have been studied previously on as-exfoliated and TFSI-treated TMDCs (*6*, *39*). The sublinear behavior of QY at high excitation levels has been attributed to a biexcitonic nonradiative recombination process and can be modeled as

$$\mathrm{QY} = \frac{\tau_r^{-1}\langle N\rangle}{\tau_r^{-1}\langle N\rangle + B_{nr}n^2 + C_{bx}\langle N\rangle^2} \quad (1)$$

where τ_r, $\langle N\rangle$, B_{nr}, C_{bx}, and n are the radiative lifetime, exciton concentration, defect-mediated nonradiative recombination rate, biexcitonic recombination coefficient, and optically generated electron concentration, respectively. For our synthetic WSe_2 monolayers after SEMD, we find that $B_{nr} = 10^4$ cm^2 s^{-1} and $C_{bx} = 0.05$ cm^2 s^{-1}. In particular, this C_{bx} value is more than 50 times lower than that of TFSI-treated MoS_2 monolayer with near-unity PL QY (*5*). The low C_{bx} value of WSe_2 is attractive, as it determines the onset of the generation rate at which the QY drop takes place, thus ultimately affecting

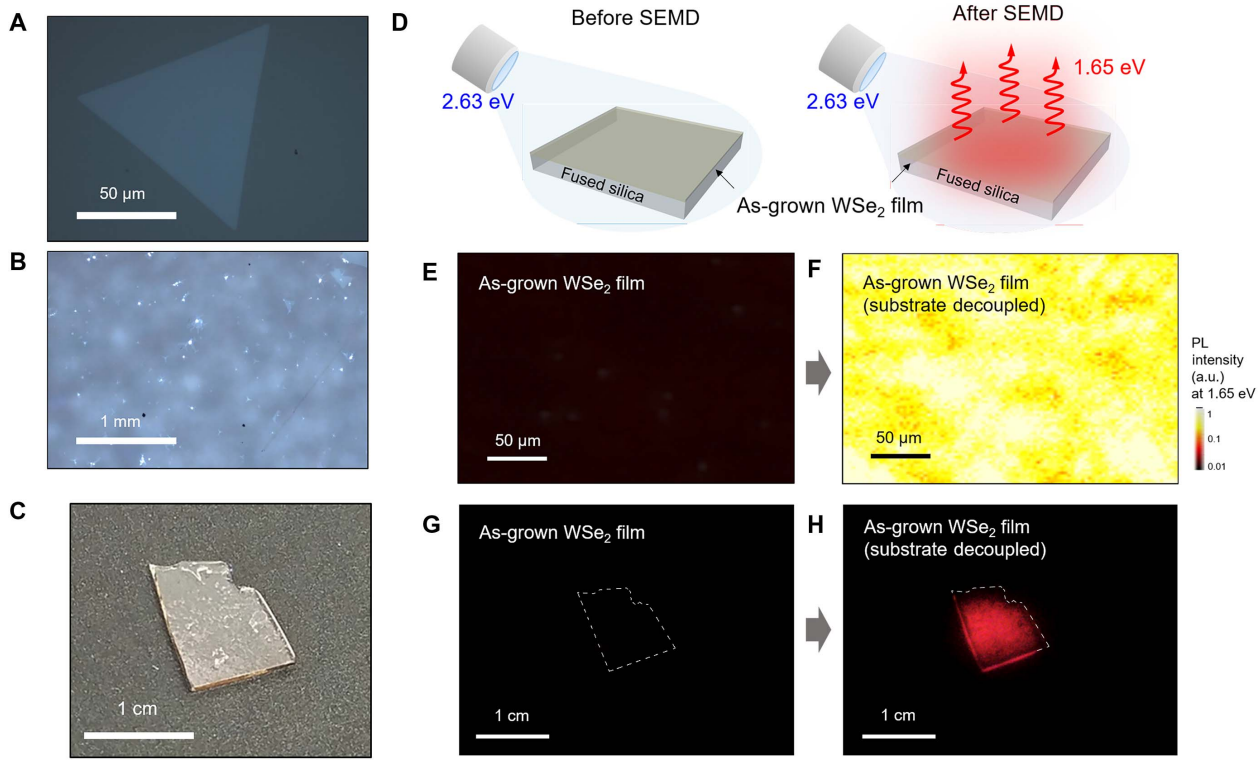

Fig. 4. Large-scale synthetic WSe_2 monolayer film with high PL QY. Optical microscopic images of (**A**) single-crystalline monolayer WSe_2 and (**B**) monolayer WSe_2 film grown on fused silica. (**C**) Photographic image of a centimeter-scale WSe_2 film sample on fused silica. (**D**) Schematic illustration describing the macroscale PL imaging of a centimeter-scale monolayer WSe_2 film on fused silica. High-magnification PL images of (**E**) as-grown and (**F**) post–SEMD process monolayer WSe_2 films. Note that the images were taken using a 1.65-eV bandpass filter that blocks the emission from the as-grown monolayer and plotted on a logarithmic scale. Macroscale PL images of a centimeter-scale grown WSe_2 film (**G**) before and (**H**) after the SEMD process. The images were taken using a commercial CMOS camera with the cold filter removed and a long-pass filter to block the excitation signal, and the power density was 0.2 W cm^{-2}.

the QY at high pump power. For light-emitting devices, the QY at high pump power is the figure of merit for projecting the efficiency, as the device is operated at high charge injection levels to achieve high brightness. We obtain a PL QY of ~12% at the high pump power of 120 W cm^{-2}, which corresponds to a generation rate of 3.5×10^{19} cm^{-2} s^{-1}. Notably, this is the highest reported PL QY at this high injection regime for TMDCs and is 20 times higher than that of TFSI-treated MoS_2 monolayer with near-unity low pump power PL QY (*5*). This presents an important advantage of WSe_2 over MoS_2 for light-emitting devices, as high current density operations can be envisioned (*24*).

Time-resolved photoluminescence (TRPL) measurements are shown in Fig. 3B and fig. S8. The extracted lifetime values are consistent with the PL QY measurement shown in Fig. 3A. In particular, for grown WSe_2 monolayers after SEMD, we observe a lifetime of 4.1 ns, while exfoliated and as-grown samples show lifetimes of 1 or sub-1 ns, respectively. In addition, we performed absorption measurements on as-exfoliated and as-grown samples and after SEMD, as shown in Fig. 3C. Consistent with previous results, we observe a shift in the A and B exciton resonances for the as-grown samples with the biaxial tensile strain, while no measurable shift is measured in the C exciton resonance (*17*, *40*), which is consistent with previous report on bending experiments (*29*). However, it should be noted that the strain was uniaxial for those experiments.

Last, we show the scalability of the growth and SEMD process by demonstrating a centimeter-scale WSe_2 monolayer film with bright PL. The growth conditions of the centimeter-scale monolayer films are specified in Materials and Methods. Figure 4 (A and B) gives representative optical microscopic images of a single-crystalline WSe_2 domain with short growth time of 20 min and monolayer film samples with longer growth time of 45 min, respectively, on fused silica. Figure 4C is a representative photograph of fused silica substrate after monolayer film growth. The monolayer film samples were excited by a blue LED with an incident power density of 0.2 W cm^{-2}, as illustrated in Fig. 4D. Using this excitation method, microscopic PL images of the WSe_2 monolayer film before and after SEMD were captured with a charge-coupled device (CCD) and are shown in Fig. 4 (E and F). The microscopic PL image shows uniformly bright PL after SEMD. Furthermore, macroscale PL imaging was performed using a commercial complementary metal-oxide semiconductor (CMOS) camera, with the cold filter removed before and after SEMD of the as-grown monolayer film. While the emission of the as-grown WSe_2 monolayer cannot be observed in this measurement configuration because of its low PL QY (Fig. 4G), the sample after SEMD results in a very strong emission from the monolayer film, as shown in Fig. 4H.

CONCLUSIONS

In summary, we demonstrate a pathway to achieve scalable WSe_2 monolayers with high PL QY for optoelectronic applications. Upon achieving the high-quality growth conditions via promoter ratio tuning, we find that the key requirement for probing the intrinsic optical property of the synthetic material is to decouple as-grown material from the substrate. We achieved this decoupling via the SEMD process. The effect of SEMD on monolayers is characterized by electron diffraction, absorption, and PL spectroscopy. As a result, we observe a PL QY of ~60% in synthetic WSe_2 monolayers, which is the highest reported value for grown TMDC monolayers and is also higher than that for mechanically exfoliated WSe_2 monolayers by an order of magnitude. The results demonstrate that, through proper material processing, TMDC monolayers with high optoelectronic quality can be obtained by direct growth over large areas.

MATERIALS AND METHODS

WSe_2 growth and transfer

The WSe_2 monolayers used in this work resemble the growth process described in detail in a previous report (*17*). However, further optimizations were made, and the WSe_2 monolayers were grown predominantly with two conditions. One growth condition was to produce single-crystalline domains ranging from 10 to 100 μm, and another growth condition was used to produce centimeter-scale monolayer WSe_2 films. Both growth processes were performed via low-pressure (~3 Torr) CVD, with presence of Ar/H_2 as the carrier gas. All WSe_2 monolayers studied in the main text were grown on a quartz substrate, except for fig. S3 (on a sapphire substrate). The substrates were previously cleaned by 10 min of sonication in acetone and isopropyl alcohol. The cleaned substrates were loaded into the downstream of the furnace. For the microscale WSe_2 samples, a ceramic boat containing a mixture of KBr and WO_3 at the weight ratio of 1:2 was placed next to the substrates, with KBr as the promoter similar to the process described in (*35*). This promoter-to-precursor weight ratio between KBr and WO_3 was tuned to optimize the growth. The used weight ratios in the manuscript were 1:2, 1:1, and 2:1. After placing another ceramic boat with Se at the upstream, the heating zones were ramped up to temperatures of 850° and 130°C, respectively, and the synthesis began with presence of H_2. The growth was performed for 20 min upon the introduction of H_2. For the WSe_2 monolayer film, a ceramic boat containing a mixture of KBr and WO_3 at the weight ratio of 1:1 was used, and the growth was done for 45 min instead of 20 min.

Optical characterization

For steady-state and transient optical characterization and calibration, the same instruments and procedures were used here as our previous study (*25*). As an excitation source, an Ar^+ laser (Lexel 95) with a 514.5-nm line was used in steady-state PL, and the power density was adjusted by neutral density filters and was simultaneously monitored by a photodiode power sensor (ThorLabs S120C). It should be noted that the ratio of laser power on the diode to incident power onto the sample was 50 so that the low laser power can be accurately measured. A 50× MD Plan (Olympus) objective lens (numerical aperture, 0.55) was used for all measurements. A Si CCD detector (Andor iDus BEX2-DD) on a spectrometer (f = 340 mm) with a grating of 150 g/mm was used to collect the steady-state PL spectra, and the dark background of the CCD was measured and subtracted each time from the acquired signal. Calibration for the external sample PL efficiency was performed using the wavelength-dependent instrument function and the collection efficiency of the instrument, which was previously described in our work (*5*). The absolute internal PL QY was extracted from the measured external quantum efficiency using the quantitative absorption at the pump wavelength and by the fraction of light within an escape cone ($1/4n^2$, where n is the refractive index of the medium). Time-resolved measurements were performed with a 514.5-nm line source (2-nm bandwidth, 20- to 30-ps pulse duration) selected from a supercontinuum laser (Fianium WhiteLase SC-400) using a double monochromator. The signal was subsequently detected using a single-photon counting avalanche photodiode (ID Quantique) with a time-correlated single-photon counting module (Becker-Hickl GmbH). In situ PL imaging was performed using the

514.5-nm Ar^+ laser, with a diffuser as an excitation source. A fluorescence microscopy setup with a 470-nm LED as an excitation source was used for the centimeter-scale film imaging, and the images were acquired using a commercial camera with 58-mm lens (*f*/5.6) after removing a cold filter where the excitation power density on the sample plane was ~0.2 W cm^{-2}. A 550-nm colored glass long-pass filter was used to block the excitation signal for PL imaging and PL spectroscopy measurements.

Transmission electron microscopy

Diffraction data were collected on an FEI Titan at 300 keV. All images, including diffraction from a polycrystalline Cu standard, were collected with the same microscope alignments. To correct for small amounts of ellipticity in the diffraction patterns due to microscope aberrations, peak positions were identified in the Cu diffraction data. A correction matrix was calculated from the elliptical fit to the points. The correction matrix was then used to determine a corrected set of image coordinates. Resampling the images according to the corrected coordinates yielded corrected images. After calculating and applying the correction to the Cu standard, the same procedure was carried out on the WSe_2 diffraction patterns.

SUPPLEMENTARY MATERIALS

Supplementary material for this article is available at http://advances.sciencemag.org/cgi/content/full/5/1/eaau4728/DC1

Fig. S1. PL imaging during the SEMD process.
Fig. S2. In situ effect of solvent immersion on the grown WSe_2 monolayer.
Fig. S3. Effect of the SEMD process on the WSe_2 monolayer grown on sapphire.
Fig. S4. Different solvents on the SEMD of the as-grown WSe_2 monolayer.
Fig. S5. TEM diffraction patterns of the WSe_2 monolayer.
Fig. S6. Effect of solvent evaporation process on the exfoliated WSe_2 monolayer.
Fig. S7. Stability of the grown WSe_2 monolayer after the SEMD process.
Fig. S8. Radiative decay curve for different WSe_2 monolayer samples.

REFERENCES AND NOTES

1. Q. H. Wang, K. Kalantar-Zadeh, A. Kis, J. N. Coleman, M. S. Strano, Electronics and optoelectronics of two-dimensional transition metal dichalcogenides. *Nat. Nanotechnol.* **7**, 699–712 (2012).
2. K. F. Mak, J. Shan, Photonics and optoelectronics of 2D semiconductor transition metal dichalcogenides. *Nat. Photonics* **10**, 216–226 (2016).
3. S. B. Desai, S. R. Madhvapathy, A. B. Sachid, J. P. Llinas, Q. Wang, G. H. Ahn, G. Pitner, M. J. Kim, J. Bokor, C. Hu, H.-S. P. Wong, A. Javey, MoS_2 transistors with 1-nanometer gate lengths. *Science* **354**, 99–102 (2016).
4. W. Zhou, X. Zou, S. Najmaei, Z. Liu, Y. Shi, J. Kong, J. Lou, P. M. Ajayan, B. I. Yakobson, J.-C. Idrobo, Intrinsic structural defects in monolayer molybdenum disulfide. *Nano Lett.* **13**, 2615–2622 (2013).
5. M. Amani, D.-H. Lien, D. Kiriya, J. Xiao, A. Azcatl, J. Noh, S. R. Madhvapathy, R. Addou, Santosh KC, M. Dubey, K. Cho, R. M. Wallace, S.-C. Lee, J.-H. He, J. W. Ager III, X. Zhang, E. Yablonovitch, A. Javey, Near-unity photoluminescence quantum yield in MoS_2. *Science* **350**, 1065–1068 (2015).
6. M. Amani, P. Taheri, R. Addou, G. H. Ahn, D. Kiriya, D.-H. Lien, J. W. Ager III, R. M. Wallace, A. Javey, Recombination kinetics and effects of superacid treatment in sulfur- and selenium-based transition metal dichalcogenides. *Nano Lett.* **16**, 2786–2791 (2016).
7. J.-G. Song, G. H. Ryu, S. J. Lee, S. Sim, C. W. Lee, T. Choi, H. Jung, Y. Kim, Z. Lee, J.-M. Myoung, C. Dussarrat, C. Lansalot-Matras, J. Park, H. Choi, H. Kim, Controllable synthesis of molybdenum tungsten disulfide alloy for vertically composition-controlled multilayer. *Nat. Commun.* **6**, 7817 (2015).
8. G. Salitra, G. Hodes, E. Klein, R. Tenne, Highly oriented WSe_2 thin films prepared by selenization of evaporated WO_3. *Thin Solid Films* **245**, 180–185 (1994).
9. Y.-H. Lee, X.-Q. Zhang, W. Zhang, M.-T. Chang, C.-T. Lin, K.-D. Chang, Y.-C. Yu, J. T.-W. Wang, C.-S. Chang, L.-J. Li, T.-W. Lin, Synthesis of large-area MoS_2 atomic layers with chemical vapor deposition. *Adv. Mater.* **24**, 2320–2325 (2012).
10. J.-K. Huang, J. Pu, C.-L. Hsu, M.-H. Chiu, Z.-Y. Juang, Y.-H. Chang,W.-H. Chang, Y. Iwasa, T. Takenobu, L.-J. Li, Large-area synthesis of highly crystalline WSe_2 monolayers and device applications. *ACS Nano* **8**, 923–930 (2014).
11. B. Liu, M. Fathi, L. Chen, A. Abbas, Y. Ma, C. Zhou, Chemical vapor deposition growth of monolayer WSe_2 with tunable device characteristics and growth mechanism study. *ACS Nano* **9**, 6119–6127 (2015).
12. S. M. Eichfeld, L. Hossain, Y.-C. Lin, A. F. Piasecki, B. Kupp, A. G. Birdwell, R. A. Burke, N. Lu, X. Peng, J. Li, A. Azcatl, S. McDonnell, R. M. Wallace, M. J. Kim, T. S. Mayer, J. M. Redwing, J. A. Robinson, Highly scalable, atomically thin WSe_2 grown *via* metal–organic chemical vapor deposition. *ACS Nano* **9**, 2080–2087 (2015).
13. K. Kang, S. Xie, L. Huang, Y. Han, P. Y. Huang, K. F. Mak, C.-J. Kim, D. Muller, J. Park, High-mobility three-atom-thick semiconducting films with wafer-scale homogeneity. *Nature* **520**, 656–660 (2015).
14. M.-Y. Li, Y. Shi, C.-C. Cheng, L.-S. Lu, Y.-C. Lin, H.-L. Tang, M.-L. Tsai, C.-W. Chu, K.-H. Wei, J.-H. He, W.-H. Chang, K. Suenaga, L.-J. Li, Epitaxial growth of a monolayer WSe_2-MoS_2 lateral p-n junction with an atomically sharp interface. *Science* **349**, 524–528 (2015).
15. K. Kang, K.-H. Lee, Y. Han, H. Gao, S. Xie, D. A. Muller, J. Park, Layer-by-layer assembly of two-dimensional materials into wafer-scale heterostructures. *Nature* **550**, 229–233 (2017).
16. M. Zhao, Y. Ye, Y. Han, Y. Xia, H. Zhu, S. Wang, Y. Wang, D. A. Muller, X. Zhang, Large-scale chemical assembly of atomically thin transistors and circuits. *Nat. Nanotechnol.* **11**, 954–959 (2016).
17. G. H. Ahn, M. Amani, H. Rasool, D.-H. Lien, J. P. Mastandrea, J. W. Ager III, M. Dubey, D. C. Chrzan, A. M. Minor, A. Javey, Strain-engineered growth of two-dimensional materials. *Nat. Commun.* **8**, 608 (2017).
18. A. McCreary, A. Berkdemir, J. Wang, M. An Nguyen, A. L. Elías, N. Perea-López, K. Fujisawa, B. Kabius, V. Carozo, D. A. Cullen, T. E. Mallouk, J. Zhu, M. Terrones, Distinct photoluminescence and Raman spectroscopy signatures for identifying highly crystalline WS_2 monolayers produced by different growth methods. *J. Mater. Res.* **31**, 931–944 (2016).
19. Y. Zhu, J. Yang, S. Zhang, S. Mokhtar, J. Pei, X. Wang, Y. Lu, Strongly enhanced photoluminescence in nanostructured monolayer MoS_2 by chemical vapor deposition. *Nanotechnology* **27**, 135706 (2016).
20. J. Kim, C. Jin, B. Chen, H. Cai, T. Zhao, P. Lee, S. Kahn, K. Watanabe, T. Taniguchi, S. Tongay, M. F. Crommie, F. Wang, Observation of ultralong valley lifetime in WSe_2/MoS_2 heterostructures. *Sci. Adv.* **3**, e1700518 (2017).
21. C. Jin, J. Kim, K. Wu, B. Chen, E. S. Barnard, J. Suh, Z. Shi, S. G. Drapcho, J. Wu, P. J. Schuck, S. Tongay, F. Wang, On optical dipole moment and radiative recombination lifetime of excitons in WSe_2. *Adv. Funct. Mater.* **27**, 1601741 (2017).
22. W. Choi, N. Choudhary, G. H. Han, J. Park, D. Akinwande, Y. H. Lee, Recent development of two-dimensional transition metal dichalcogenides and their applications. *Mater. Today* **20**, 116–130 (2017).
23. Y. Ye, Z. J. Wong, X. Lu, X. Ni, H. Zhu, X. Chen, Y. Wang, X. Zhang, Monolayer excitonic laser. *Nat. Photonics* **9**, 733–737 (2015).
24. D.-H. Lien, M. Amani, S. B. Desai, G. H. Ahn, K. Han, J.-H. He, J. W. Ager III, M. C. Wu, A. Javey, Large-area and bright pulsed electroluminescence in monolayer semiconductors. *Nat. Commun.* **9**, 1229 (2018).
25. H. Kim, D.-H. Lien, M. Amani, J. W. Ager, A. Javey, Highly stable near-unity photoluminescence yield in monolayer MoS_2 by fluoropolymer encapsulation and superacid treatment. *ACS Nano* **11**, 5179–5185 (2017).
26. M. Amani, R. A. Burke, X. Ji, P. Zhao, D.-H. Lien, P. Taheri, G. H. Ahn, D. Kirya, J. W. Ager III, E. Yablonovitch, J. Kong, M. Dubey, A. Javey, High luminescence efficiency in MoS_2 grown by chemical vapor deposition. *ACS Nano* **10**, 6535–6541 (2016).
27. Z. Liu, M. Amani, S. Najmaei, Q. Xu, X. Zou, W. Zhou, T. Yu, C. Y. Qiu, A. G. Birdwell, F. J. Crowne, R. Vajtai, B. I. Yakobson, Z. Xia, M. Dubey, P. M. Ajayan, J. Lou, Strain and structure heterogeneity in MoS_2 atomic layers grown by chemical vapour deposition. *Nat. Commun.* **5**, 5246 (2014).
28. G. Plechinger, A. Castellanos-Gomez, M. Buscema, H. S. J. van der Zant, G. A. Steele, A. Kuc, T. Heine, C. Schüller, T. Korn, Control of biaxial strain in single-layer molybdenite using local thermal expansion of the substrate. *2D Mater.* **2**, 015006 (2015).
29. S. B. Desai, G. Seol, J. S. Kang, H. Fang, C. Battaglia, R. Kapadia, J. W. Ager, J. Guo, A. Javey, Strain-induced indirect to direct bandgap transition in multilayer WSe_2. *Nano Lett.* **14**, 4592–4597 (2014).
30. J. Choi, H. Zhang, H. Du, J. H. Choi, Understanding solvent effects on the properties of two-dimensional transition metal dichalcogenides. *ACS Appl. Mater. Interfaces* **8**, 8864–8869 (2016).
31. Z. Cao, A. V. Dobrynin, Polymeric droplets on soft surfaces: From Neumann's triangle to Young's law. *Macromolecules* **48**, 443–451 (2015).
32. N. Nadermann, C.-Y. Hui, A. Jagota, Solid surface tension measured by a liquid drop under a solid film. *Proc. Natl. Acad. Sci. U.S.A.* **110**, 10541–10545 (2013).
33. C.-Y. Hui, A. Jagota, Planar equilibrium shapes of a liquid drop on a membrane. *Soft Matter* **11**, 8960–8967 (2015).

34. R. D. Schulman, K. Dalnoki-Veress, Liquid droplets on a highly deformable membrane. *Phys. Rev. Lett.* **115**, 206101 (2015).
35. S. Li, S. Wang, D.-M. Tang, W. Zhao, H. Xu, L. Chu, Y. Bando, D. Golberg, G. Eda, Halide-assisted atmospheric pressure growth of large WSe_2 and WS_2 monolayer crystals. *Appl. Mater. Today* **1**, 60–66 (2015).
36. P. Schmidt, M. Binnewies, R. Glaum, M. Schmidt, Chemical Vapor Transport Reactions -Methods, Materials, Modeling, in *Advanced Topics on Crystal Growth*, S. O. Ferreira, Ed. (InTech, 2013).
37. P. Johari, V. B. Shenoy, Tuning the electronic properties of semiconducting transition metal dichalcogenides by applying mechanical strains. *ACS Nano* **6**, 5449–5456 (2012).
38. Y. Yu, G. Li, L. Huang, A. Barrette, Y. Q. Cai, Y. Yu, K. Gundogdu, Y. W. Zhang, L. Cao, Enhancing multifunctionalities of transition-metal dichalcogenide monolayers *via* cation intercalation. *ACS Nano* **11**, 9390–9396 (2017).
39. A. J. Goodman, A. P. Willard, W. A. Tisdale, Exciton trapping is responsible for the long apparent lifetime in acid-treated MoS_2. *Phys. Rev. B* **96**, 121404 (2017).
40. Y. Li, A. Chernikov, X. Zhang, A. Rigosi, H. M. Hill, A. M. van der Zande, D. A. Chenet, E.-M. Shih, J. Hone, T. F. Heinz, Measurement of the optical dielectric function of monolayer transition-metal dichalcogenides: MoS_2, $MoSe_2$, WS_2, and WSe_2. *Phys. Rev. B* **90**, 205422 (2014).

Acknowledgments: We thank S. B. Desai for the helpful discussions. **Funding:** Materials growth, characterization, and modeling were supported by the Electronic Materials Program funded by the Director, Office of Science, Office of Basic Energy Sciences, Materials Sciences and Engineering Division of the U.S. Department of Energy, under contract no. DE-AC02-05CH11231. Electron microscopy was performed at the Molecular Foundry, which was supported by the Office of Science, Office of Basic Energy Sciences of the U.S. Department of Energy under contract no. DE-AC02-05CH11231. H.K. acknowledges the support from a Samsung Scholarship. A.J. acknowledges the support from Lam Research. **Author contributions:** H.K. and G.H.A. designed the concepts, performed the experiments, and analyzed the data. J.C. helped with the synthesis of the samples. M.A. built the measurement setup and helped with the in situ PL spectroscopy. J.P.M. carried out the simulations. C.K.G. and M.C.S. performed the TEM measurements. D.-H.L., Y.Z., and J.W.A. advised on the experiments. D.C.C. helped with the data analysis and proposed the model for the mechanism. A.J. directed the research. H.K., G.H.A., and A.J. wrote the manuscript. All authors read and contributed to the preparation of the manuscript. **Competing interests:** The authors declare that they have no competing interests. **Data and materials availability:** All data needed to evaluate the conclusions in the paper are present in the paper and/or the Supplementary Materials. Additional data related to this paper may be requested from the authors.

Submitted 14 June 2018
Accepted 28 November 2018
Published 2 January 2019
10.1126/sciadv.aau4728

Citation: H. Kim, G. H. Ahn, J. Cho, M. Amani, J. P. Mastandrea, C. K. Groschner, D.-H. Lien, Y. Zhao, J. W. Ager III, M. C. Scott, D. C. Chrzan, A. Javey, Synthetic WSe_2 monolayers with high photoluminescence quantum yield. *Sci. Adv.* **5**, eaau4728 (2019).

ScienceAdvances

Synthetic WSe_2 monolayers with high photoluminescence quantum yield

Hyungjin Kim, Geun Ho Ahn, Joy Cho, Matin Amani, James P. Mastandrea, Catherine K. Groschner, Der-Hsien Lien, Yingbo Zhao, Joel W. Ager III, Mary C. Scott, Daryl C. Chrzan and Ali Javey

Sci Adv **5** (1), eaau4728.
DOI: 10.1126/sciadv.aau4728